

Spherical-harmonic-analysis-based optimization of atomic weighting functions for multicenter numerical integration in molecules

Dimitri N. Laikov^{1, a)}

Chemistry Department, Moscow State University, 119991 Moscow, Russia

The well-known spatial integration schemes in molecular electronic structure theory, immune to cusps and point singularities of some kind at atomic positions, use a set of weighting functions to split the integrand into a sum of atom-centered parts, each dealt with in its own spherical coordinate system. Here, for a given set of integrands in the two-center case, a quality measure of the weighting functions is defined to compare, design, and optimize them, it is roughly proportional to the average number of angular quadrature points needed to reach a given integration accuracy. A study of Becke's fuzzy Voronoi cells has helped to improve their performance by a new modification. New spherically-symmetric unnormalized weighting functions are found in the form of a negative power times the negative exponential of the fourth power of the scaled distance to the atomic center, with the parameters related to the asymptotic decay of the integrand and the integration accuracy — these are much simpler but no less efficient and naturally fit for linear-scaling calculations. Radial distribution of spherical quadrature orders is studied. A radial integration scheme of double exponential type is optimized. A symmetric analog of the pseudospectral approximation is used for the seminumerical evaluation of two-electron repulsion integrals. Taken together, this allows efficient calculation of all molecular integrals with well-controlled accuracy, as shown by tests on a set of molecules.

I. INTRODUCTION

Three-dimensional numerical integration is a helpful tool for molecular electronic structure calculations: on one hand, it is the best and almost the only way to deal with the exchange-correlation models of density functional¹ theory; on the other hand, even when the analytic solutions are known, it can greatly speed up the evaluation of the direct and exchange two-electron terms²⁻⁶ of wavefunction methods, and even the many-electron integrals^{7,8} of explicitly correlated approaches; furthermore, it is highly vectorizable and parallelizable. The multicenter nature of the integrand, that may have cusps or point singularities at each atomic center, makes the design of a good cubature rule for polyatomic molecules more than a worthwhile mathematical exercise. Two main paths have been followed: a division of space into atomic spheres and interstitial regions⁹, without overlap, each with its own grid of points; or the use of atomic weighting functions to split^{10,11} the integrand into a sum of well-behaved overlapping atom-centered functions, each of which is dealt with in its own spherical coordinate system. It is the latter that we study here, the main idea was born¹⁰ when the computational chemistry was in its childhood, but 22 years later it began to grow into a heavy-load workhorse after the fuzzy Voronoi¹² cells were used to build¹¹ the now-standard weighting functions — despite their formal cubic scaling, they were quickly adapted¹³ for linear-scaling calculations, a more detailed study¹⁴ has later shown how to overcome their limitations more carefully with accuracy in mind. For periodic systems, spherical (unnormalized) weighting functions in the form of inverse third power times negative

exponential of the distance have been reported¹⁵ to work, and yet another form¹⁶ of this kind has long been used for isolated systems.

It is natural to ask whether there is some best form of the atomic weighting functions and how to find it. Here, we find an answer by understanding that it is the angular integration that determines the performance — with an adaptive¹⁷ choice of the order of quadratures^{18,19} for each spherical shell to meet a given integration accuracy, it is the number of angular points that grows the fastest and is most sensitive to the integrand's behavior. As there is no well-defined orientation of the spherical grids that could always smoothly follow the changes in molecular geometry, a rather high accuracy may often be needed to get rotationally-invariant molecular energies and their derivatives free of random noise. We take the two-center (diatomic) case as a model, define a measure of the weighting functions' fitness, and use it to design and optimize them — a sound scheme should then work in the general polyatomic case as well and can be tested on realistic systems.

Beside the weighting functions, a fully-fledged molecular integration scheme also needs a radial distribution of spherical quadrature orders around each atom and a good radial quadrature itself. We find an analytic fit to the distribution of orders in the diatomic case and use it to make a geometry-dependent polyatomic generalization that is more economical than the traditional pruning²⁰. A number of radial grids^{11,21-23} are in widespread use, the idea of double-exponential²⁴ integration has also found its way²⁵ into this field — here, we have further optimized one such scheme and derived the estimates of its accuracy and convergence.

^{a)} laikov@rad.chem.msu.ru; <http://rad.chem.msu.ru/~laikov/>

II. METHODOLOGY

Let $\{\mathbf{R}_i\}$ be the atomic positions in a molecule, but we will first study a *diatomic* fragment with its cylindrically-symmetric weighting function

$$w_{ij}(\mathbf{r}) = w(|\mathbf{r} - \mathbf{R}_i|, |\mathbf{r} - \mathbf{R}_j|, |\mathbf{R}_i - \mathbf{R}_j|) \quad (1)$$

as a starting for polyatomic generalizations. The function $w(r_i, r_j, R) \geq 0$ of the three distances should have the properties

$$w(r_i, r_j, R) + w(r_j, r_i, R) = 1, \quad (2)$$

$$w(0, R, R) = 1, \quad (3)$$

$$w(R, 0, R) = 0, \quad (4)$$

and its best form is to be found. A good $w(r_i, r_j, R)$ should be localized around $r_i = 0$ and suppress singularities of the integrands as $r_j \rightarrow 0$ of the kind up to r_j^{-2} , and the smoother the better.

We make a set of $2N$ model test functions

$$f_n(r_i, r_j, R) = \begin{cases} w(r_i, r_j, R)b_n(r_i), & 0 \leq n < N, \\ w(r_i, r_j, R)b_{n-N}(r_j), & N \leq n < 2N, \end{cases} \quad (5)$$

with the normalized radial parts

$$b_n(r) = \frac{\alpha_n^3}{\pi^{3/2}} \exp(-\alpha_n^2 r^2) \quad (6)$$

and densely-spaced even-tempered exponents

$$\alpha_n = \alpha \cdot 2^{n/M}, \quad (7)$$

this is a fairly good model of a whole set of two-center molecular integrands, simplified by dropping the low-order polynomial factors that are too well-behaved to play a big role in what follows. We take $M = 16$ in Eq. (7) which is more than enough, $M = 8$ is almost as good. In all cases studied, $\alpha_n > 2^6$ make zero contribution, so we work with the sets $\alpha \leq \alpha_n \leq 2^6$ having only one parameter α .

As the weighting function $w(r_i, r_j, R)$ will be optimized for the integration in spherical coordinates centered at $r_i = 0$, we get first the coefficients from the spherical harmonic analysis

$$A_{ln}(r, R) = \int_{-1}^1 \bar{P}_l(z) f_n\left(r, \sqrt{r^2 - 2Rrz + R^2}, R\right) dz, \quad (8)$$

made simple thanks to the cylindrical symmetry of the problem, using the normalized Legendre polynomials

$$\bar{P}_l(z) = \sqrt{l + \frac{1}{2}} P_l(z), \quad (9)$$

$$P_0(z) = 1, \quad (10)$$

$$P_1(z) = z, \quad (11)$$

$$lP_l(z) = (2l - 1)zP_{l-1}(z) - (l - 1)P_{l-2}(z). \quad (12)$$

A Gauß–Legendre quadrature of a high enough order can be used to integrate numerically over z in Eq. (8), but the highest precision and fastest convergence can be reached by a double-exponential²⁴ integration, we change the variable

$$z = \tanh\left(\frac{2\sqrt{3}}{\sqrt{4-\pi}} \cdot \frac{x}{1-x^2}\right) \quad (13)$$

and apply the trapezoidal rule for $-1 < x < 1$.

A (hopefully exponential) convergence of $|A_{ln}|$ as $l \rightarrow \infty$ can be quantified by the residuals

$$Q_{Ln}(r, R) = 2\pi r^3 \cdot \left(\sum_{l=L}^{\infty} A_{ln}^2(r, R)\right)^{1/2}, \quad (14)$$

that can also be computed as

$$Q_{Ln}(r, R) = 2\pi r^3 \cdot \left(B_n(r, R) - \sum_{l=0}^{L-1} A_{ln}^2(r, R)\right)^{1/2}, \quad (15)$$

$$B_n(r, R) = \int_{-1}^1 f_n^2\left(r, \sqrt{r^2 - 2Rrz + R^2}, R\right) dz. \quad (16)$$

For lower-precision work, we use the more stable Eq. (14) together with the Gauß–Legendre rule for Eq. (8); for arbitrary precision computation, however, we use Eqs. (15) and (16) together with the double-exponential integration over z through Eq. (13) in both Eqs. (8) and (16).

The greatest value over the test functions

$$Q_L(r, R) = \max_n Q_{Ln}(r, R) \quad (17)$$

is a measure of how well the weighting functions work. Instead of picking up the greatest value from the set of $2N$, however dense it may be, a full maximization of $Q_{Ln}(r, R)$ with respect to $\alpha_n \geq \alpha$ in Eq. (6) can be done numerically to reach the limit of Eq. (17) as $N, M \rightarrow \infty$, we do so when we need the highest precision.

To simplify the optimization, a continuous function is made from the discrete values of $Q_L(r, R)$ through the piecewise linear interpolation

$$Q(L, r, R) = (L - [L]) (Q_{[L+1]}(r, R) - Q_{[L]}(r, R)) + Q_{[L]}(r, R), \quad (18)$$

the inverse function $\mathcal{L}(r, R, \varepsilon) \geq 0$ can then be found from

$$Q(\mathcal{L}(r, R, \varepsilon), r, R) = \varepsilon, \quad (19)$$

meaning the order of angular quadrature needed to integrate all test functions to within a given error tolerance ε . We define our objective function

$$\mathcal{N}(R, \varepsilon) = \sum_{k=-\infty}^{+\infty} \mathcal{N}(r_k, R, \varepsilon) d_k, \quad (20)$$

$$\mathcal{N}(r, R, \varepsilon) = \left[\max(\mathcal{L}(r_k, R, \varepsilon), l) + 1 \right]^2 - (l + 1)^2, \quad (21)$$

as roughly proportional to the number of angular integration points (beyond order l , we set $l = 1$) on all spherical shells for $0 \leq r < \infty$, and a further average

$$\mathcal{M}(\varepsilon) = \sum_{k=0}^{\infty} \mathcal{N}(R_k, \varepsilon) D_k \quad (22)$$

over all $R_0 \leq R < \infty$, with a simple discretization

$$r_k = 2^{(k+t)/K}, \quad d_k = (\ln 2)/K \quad (23)$$

(we set $t = 0$ for now, but will vary it later),

$$R_k = R_0 \cdot 2^{k/K}, \quad D_k = R_0 \cdot (\ln 2)/K, \quad (24)$$

and a natural $R_0 = 1$ au. The sum in Eq. (20) is only formally infinite since for both $k \ll -K$ and $k \gg K$ all terms go quickly to zero (with $l = 1$ in Eq. (21), but with $l = 0$ the convergence would have been too slow), and the same is true for Eq. (22). We take $K = 16$ in both Eqs. (23) and (24) that is enough to integrate the functions to about 36 bits of precision.

Both $\mathcal{N}(R, \varepsilon)$ of Eq. (20) and $\mathcal{M}(\varepsilon)$ of Eq. (22) are functionals of the weighting function $w(r_i, r_j, R)$ — through Eqs. (5), (8), (14), (17), (18), and (19) — and their minimization leads to its optimal form for a given or all R .

After the weighting function has been determined, it is time to study the convergence of radial integrals over r , for which the even-tempered scheme of Eq. (23) is natural thanks to its self-similarity. From Eq. (8), the sums

$$\tilde{S}_n(R, t, K) = \sqrt{2} \sum_{k=-\infty}^{+\infty} A_{0n}(r_k, R) d_k \quad (25)$$

add up to make N approximate integrals

$$\bar{S}_n(R, t, K) = \tilde{S}_n(R, t, K) + \tilde{S}_{N+n}(R, t, K) \approx 1 \quad (26)$$

of the normalized functions of Eq. (6), and depend on the point density K and the shift t . The integration error

$$\mathcal{E}_n(R, K) = \max_{0 \leq t \leq 1} |\bar{S}_n(R, t, K) - 1| \quad (27)$$

can be further condensed to

$$\mathcal{E}(R, K) = \max_n \mathcal{E}_n(R, K) \quad (28)$$

and even

$$\mathcal{E}(K) = \max_{R_0 \leq R < \infty} \mathcal{E}(R, K). \quad (29)$$

Most often, $\mathcal{E}(R, K)$ is greatest at $R = R_0$, and it is enough to work only with $\mathcal{E}(R_0, K)$, so we define the function $K(\varepsilon)$ implicitly,

$$\mathcal{E}(R_0, K(\varepsilon)) = \varepsilon, \quad (30)$$

as the (logarithmic) radial point density needed to reach the integration accuracy ε .

We could have also considered the product $K(\varepsilon) \cdot \mathcal{M}(\varepsilon)$ as a measure of both radial and angular integration cost to be minimized, but we put it aside.

We begin our numerical studies with the well-known¹¹ weighting functions of the kind

$$w(r_i, r_j, R) = w_p \left(\frac{r_i - r_j}{\varrho(R)} \right), \quad (31)$$

where the simplest smooth step function

$$w_p(x) = \begin{cases} 1, & x < -1, \\ \frac{1}{2} - \frac{1}{2} s_p(x), & -1 \leq x \leq 1, \\ 0, & x > 1, \end{cases} \quad (32)$$

is made from the shifted p -times iterated polynomial

$$s_p(x) = \frac{3}{2} s_{p-1}(x) - \frac{1}{2} s_{p-1}^3(x), \quad (33)$$

$$s_0(x) = x. \quad (34)$$

For the distance scale function $\varrho(R)$, the simplest¹¹ case $\varrho(R) = R$ can be compared to the newer¹⁴ cut-off version

$$\varrho(R) = \min(R, c) \quad (35)$$

with some c . For $2^{-4} \leq \alpha \leq 2^{-2}$ and $2^{-24} \leq \varepsilon \leq 2^{-16}$ we have optimized this c and found a fit

$$c = C/\alpha \quad (36)$$

with $C \approx 1.5$ for $p = 3$ and $C \approx 3.0$ for $p = 4$, C also being a weak and irregular function of ε . Fig. 1 shows a typical example where we see how Eq. (35) helps to overcome the shortcomings of the simplest $\varrho(R) = R$, strongly for $p = 3$, but less so for $p = 4$.

For $p = 3$, we have also optimized the values of $\varrho(R)$ for $\mathcal{N}(R, \varepsilon)$ at each R_k of Eq. (24) and found them to fit well to a two-parameter function

$$\varrho(R) = c \left[1 - \exp \left(-\frac{bR}{c} - \frac{b^2 R^2}{2c^2} \right) \right] \quad (37)$$

with $b \approx 0.9$ and c following Eq. (36) with $C \approx 2.0$ for all α and ε studied. Fig. 1 shows a further lowering and now a smooth curve, this seems to be the best one can get from Eq. (31). For $p = 4$, Eq. (37) tends to an unsafe $b > 1$, and when constrained to $b = 1$, there is only a slight change from what Eq. (35) yields.

Higher derivative discontinuity of $w_p(x)$ at $x = \pm 1$ made us think of fully differentiable analogs, we have tested

$$\bar{s}_p(x) = \tanh \left(\frac{3^p}{2^p} \cdot \frac{x}{1 - x^2} \right), \quad (38)$$

which mimics $s_p(x)$ but is not limited to an integer p — even with the optimized p , however, it worked only slightly worse than the original $s_p(x)$ of Eq. (33).

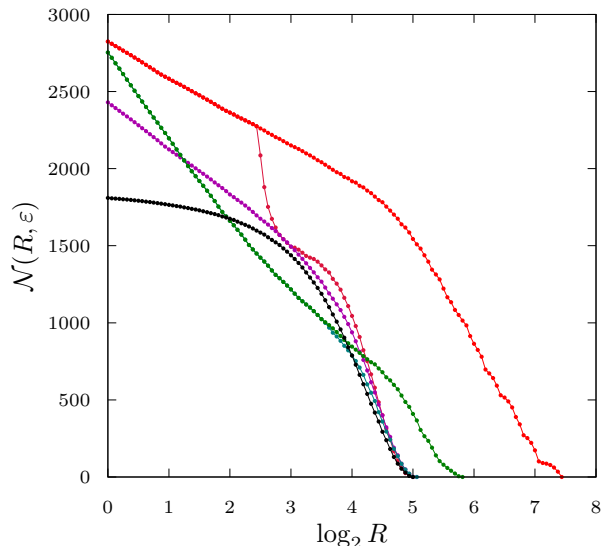


FIG. 1. Functional $\mathcal{N}(R, \varepsilon)$ of Eq. (20) computed over: $w_3(x)$ of Eq. (32) with (red) $\varrho(R) = R$, (crimson) Eq. (35), and (purple) Eq. (37); $w_4(x)$ of Eq. (32) with (green) $\varrho(R) = R$ and (teal) Eq. (35); (black) $u(r)$ of Eq. (40) with $\mu = 4$, $\nu = 8$. $\log_2 \alpha = -2$ and $\log_2 \varepsilon = -20$ everywhere.

Another kind¹⁰ of weighting function

$$w(r_i, r_j) = \frac{u(r_i)}{u(r_i) + u(r_j)} \quad (39)$$

is made from an unnormalized spherically-symmetric distribution $u(r) \geq 0$, we tried a number of them until we have found a good and simple analytical form

$$u(r) = \frac{1}{r^\nu} \exp\left(-\left(\frac{r}{\sigma}\right)^\mu\right) \quad (40)$$

with an optimized length scale σ . Seeking the best μ and ν among integers, we have settled on $\mu = 4$ (although $\mu = 6$ worked as well) and then believed that $\nu = 8$ would have been right also. Strikingly, as seen in Fig. 1, all this yields $\mathcal{N}(R, \varepsilon)$ that is smooth and everywhere lower than the best we can get from Eq. (31)!

Further tests have shown, however, that ν should be a function of at least ε lest there be too fast a growth of $\mathcal{L}(r, R, \varepsilon)$ as $\varepsilon \rightarrow 0$ at and near $r = R$, that is when the sphere passes through the other center. To find our best $\nu(\varepsilon)$, we minimize $Q_L(1, 1)$ of Eq. (17) with respect to ν , using Eqs. (39) and (40) with $\sigma = \infty$, for $L = 8, \dots, 192$ and so we get a table of pairs (ε_L, ν_L) shown in Fig. 2. A simple function

$$\nu(\varepsilon) = \kappa \cdot (\eta - \log_2 \varepsilon)^\zeta \quad (41)$$

fits these data well, the parameters $\kappa \approx 0.748$, $\eta \approx 12.0$, and $\zeta \approx 0.71$ can be determined to only a few digits because there seems to be a random noise-like component, but this is enough as seen in Fig. 2. With $\nu(\varepsilon)$ of

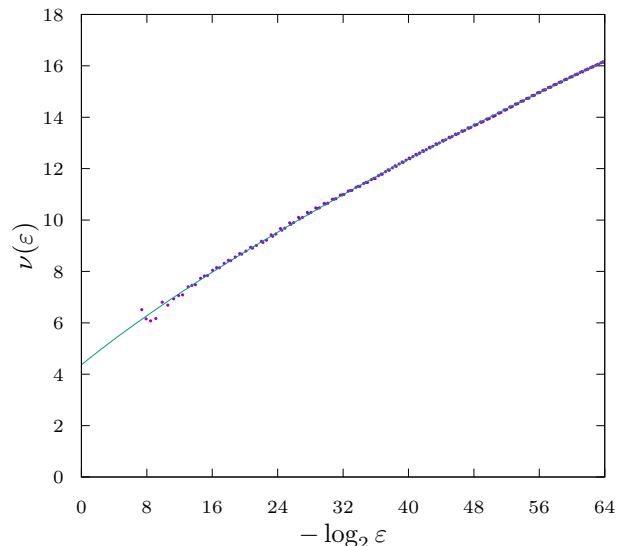


FIG. 2. Function $\nu(\varepsilon)$ as computed numerically (dots) and its approximation (solid line) of Eq. (41).

Eq. (41) at hand, we optimize σ in Eq. (40) for the ranges $2^{-4} \leq \alpha \leq 2^{-2}$ and $2^{-32} \leq \varepsilon \leq 2^{-16}$, and we find a good fit to the data with

$$\sigma(\alpha, \varepsilon) = \frac{\sqrt{\beta - \gamma \log_2 \varepsilon}}{\alpha} \quad (42)$$

and the parameters $\beta \approx 1.32$ and $\gamma \approx 0.38$ safely rounded. Thus we get our best weighting function of Eqs. (40), (41), and (42).

The multicenter¹¹ generalization of Eq. (31) uses the intermediate products

$$P_i(\mathbf{r}) = \prod_{j \neq i} w_{ij}(\mathbf{r}), \quad (43)$$

the so-called fuzzy Voronoi cell functions, from which the atomic weights are made,

$$W_i(\mathbf{r}) = \frac{P_i(\mathbf{r})}{\sum_j P_j(\mathbf{r})}, \quad (44)$$

without cut-offs, their computational cost grows cubically with the number of atoms. At the same time, Eq. (39) readily generalizes into the simplest form,

$$W_i(\mathbf{r}) = \frac{u(|\mathbf{r} - \mathbf{R}_i|)}{\sum_j u(|\mathbf{r} - \mathbf{R}_j|)}, \quad (45)$$

growing at most quadratically, making it once again our best scheme. Using cut-offs, both schemes reach a linear scaling, but the latter should have a sooner onset and a much smaller prefactor.

Now we need a way to assign the orders $L_i(r)$ of spherical quadrature rules at distance r around each center i in a polyatomic environment, they should be no less than

$$L_i^0 = 4l_i + l_d, \quad (46)$$

l_i being the highest angular momentum of basis functions on the i -th atom, and l_d the order of derivatives (if any). Starting from the two-center distribution $L(r, R, \alpha, \varepsilon)$, a rounded up integer version of $\mathcal{L}(r, R, \varepsilon)$ from Eq. (19), to which we make a simple analytic fit in Appendix A as shown in Fig. 3, we try to find a multicenter generalization of diatomic fragment functions

$$L_{ij}(r) = L(r, |\mathbf{R}_i - \mathbf{R}_j|, \alpha, \varepsilon) \quad (47)$$

first in the form

$$\bar{L}_i(r) = \max(L_i^0, \max_{j \neq i} L_{ij}(r)), \quad (48)$$

in other words, $L_{ij}(r)$ is the influence of j -th atom on $L_i(r)$, and the greatest value is taken. We see in Fig. 3 the peaks around $r \approx R$, they should be even sharper for $(L_i(r) + 1)^2$, so it would have been a waste to work with the good-for-all- R solution

$$\tilde{L}_i(r) = \max(L_i^0, \max_{R > R_0} L(r, R, \alpha, \varepsilon)), \quad (49)$$

and we were optimistic about Eq. (48) for some time. Polyatomic tests have later shown, however, that the influences are not independent and a higher $L_i(r)$ is needed when the other atoms are crowding around. We find a quick fix to this problem,

$$L_i(r) = \bar{L}_i(r) \cdot \theta \left(\frac{\bar{M}_i(r)}{(\bar{L}_i(r) + 1)^2} - 1 \right), \quad (50)$$

$$\bar{M}_i(r) = (L_i^0 + 1)^2 + \sum_{j \neq i} \left((L_{ij}(r) + 1)^2 - 1 \right), \quad (51)$$

$$\theta(x) = 1 + \beta \cdot (1 - \exp(-\gamma x)), \quad (52)$$

the parameters $\beta \approx \frac{1}{2}$ and $\gamma \approx 1$ can be adjusted to get $L_i(r)$ high enough, but often too much. Thus, a straightforward assignment of quadrature orders can hardly be as good as we wanted (but we had to have studied it before saying so!), and we have therefore worked out a new fully adaptive method (given below) of the old¹⁷ kind.

In the end, we need a better radial integration scheme than in Eq. (23). We have optimized not just one²⁵ but the two parameters p and q in the mapping

$$r = \frac{1}{A} \exp(x - q \exp(-px)) \quad (53)$$

of the distance r onto the dimensionless variable x in the range $-\infty < x < \infty$, so that the trapezoidal rule

$$x_k = x_0 + kh \quad (54)$$

works well (with cut-offs at both ends) for a set of functions of Eq. (6) with $\alpha_n \leq A$, and for any x_0 . A good solution is $p = 2$, $q = \frac{1}{8}$, a detailed derivation is given in

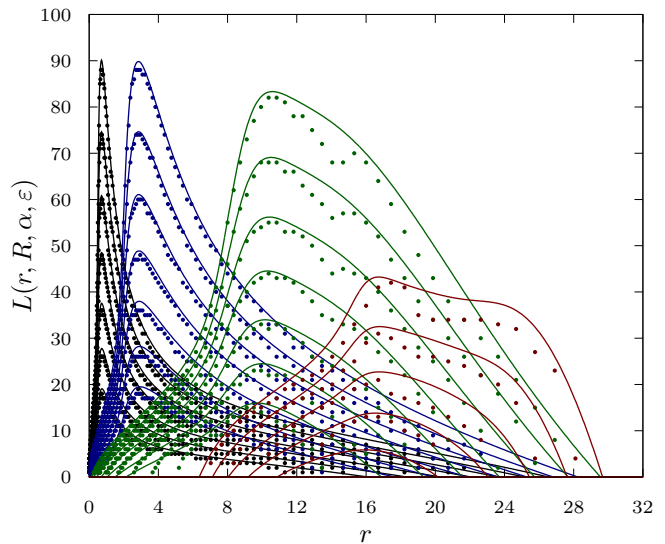


FIG. 3. Distribution of spherical quadrature orders (dots) and its approximation $L(r, R, \alpha, \varepsilon)$ of Appendix A, unrounded (lines), for $\log_2 \alpha = -2$; $-\log_2 \varepsilon = 12, 16, 20, 24, 28, 32, 36$; and $R = 1, 4, 16, 32$ (black, blue, green, red).

Appendix B together with the convergence properties as $h \rightarrow 0$. Setting $x_0 = \ln A$, we get the quadrature roots and weights

$$\begin{cases} r_k = \exp(hk - q \exp(-p(hk + \ln A))), \\ d_k = (1 + pq \exp(-p(hk + \ln A)))h, \end{cases} \quad (55)$$

which for $h = (\ln 2)/K$ is a tailored version of the ‘‘half double-exponential’’ scheme of Eq. (23), and a radial integral is computed as

$$\int_0^\infty r^2 f(r) dr \approx \sum_{k=k_0}^{k_1} r_k^3 f(r_k) d_k. \quad (56)$$

The inner cut-off k_0 is clearly set by

$$\frac{A^3}{\pi^{3/2}} r_{k_0}^2 d_{k_0} \approx \varepsilon, \quad (57)$$

(we aim it at the functions $b_n(r)$ of Eq. (6) and also at $r^{-1}b_n(r)$ as a model of Coulomb integrals, hence $r_{k_0}^2$), while for the outer,

$$r_{k_1} \approx r_1(\varepsilon), \quad (58)$$

we have to study (for our best weighting function) how far r_k should reach to converge the sum in Eq. (25) to within $\varepsilon_1 \approx \frac{1}{4}\varepsilon$, for all R , and we compute a table of values that can be fitted well by the function

$$r_1(\varepsilon) = \frac{1}{\alpha} \left[\beta + \frac{\kappa}{\gamma} \ln \left(1 + \exp(\gamma(\eta - \log_2 \varepsilon)) \right) \right] \quad (59)$$

with the parameters $\beta \approx 4.38$, $\kappa \approx 0.123$, $\gamma \approx 0.6$, and $\eta \approx -15.0$, we see that $r_1(\varepsilon)$ stretches beyond the range

of functions on the first center to reach what the weighting function has not fully suppressed on the other.

Solving Eq. (30) with $R_0 = 1$ numerically, a table of $K(\varepsilon)$ values for $6 \leq -\log_2 \varepsilon \leq 36$ is computed and can be fitted well by the function

$$K(\varepsilon) = \beta + \kappa \cdot (\eta - \log_2 \varepsilon)^\zeta \quad (60)$$

with parameters $\beta \approx 0.91$, $\kappa \approx 0.0608$, $\eta \approx -4.2$, and $\zeta \approx 1.59$, the functions on the other center do make the radial integration more of a challenge even with the best weighting function we have, this $K(\varepsilon)$ is up to a few times higher than in the ideal one-center case of Eq (B20).

So we set the range and density of integration points by Eqs. (57), (58), (59), and (60).

Working with the traditional atomic basis functions

$$\chi_{mlni}(\mathbf{r}) = Y_{lm} \left(\frac{\mathbf{r} - \mathbf{R}_i}{|\mathbf{r} - \mathbf{R}_i|} \right) f_{nli}(|\mathbf{r} - \mathbf{R}_i|) \quad (61)$$

of Gaussian²⁶ type, with the radial parts

$$f_{nli}(r) = r^l \sum_p c_{pnl} \exp(-a_{pli} r^2), \quad (62)$$

and the exponent range

$$a_i^{\min} \leq a_{pli} \leq a_i^{\max}, \quad (63)$$

we set

$$A_i = \sqrt{2a_i^{\max}} \quad (64)$$

in Eqs. (55) and (57) for each atom i , while a global value

$$\alpha = \sqrt{2 \min_i a_i^{\min}} \quad (65)$$

is taken for all atoms in the system. (We remember that the ‘‘atomic size adjustments’’¹¹ have also been dropped from later works.)

Putting everything together, we get the positions $\{\mathbf{r}_{mki}\}$ and weights $\{w_{mki}\}$ of the multicenter spatial cubature

$$\mathbf{r}_{mki} = \mathbf{r}_{mLki}, \quad (66)$$

$$w_{mki} = w_{mLki}, \quad (67)$$

$$\mathbf{r}_{mLki} = \mathbf{R}_i + \mathbf{X}_i \mathbf{u}_{mL} r_{ki}, \quad (68)$$

$$w_{mLki} = 4\pi s_{mL} r_{ki}^3 W_i(\mathbf{r}_{mLki}) d_k, \quad (69)$$

$$L_{ki} \equiv L_i(r_{ki}), \quad (70)$$

where $\{\mathbf{u}_{mL}\}$ are the positions and $\{s_{mL}\}$ the weights of a quadrature^{18,19} of order L on the unit sphere. For each atom, the spherical grids are aligned with the principal axes \mathbf{X}_i of an inertia-like tensor

$$\mathbf{Y}_i = \sum_{j \neq i} \mathbf{Y}(\mathbf{R}_j - \mathbf{R}_i, \alpha), \quad (71)$$

$$\mathbf{Y}(\mathbf{r}, \alpha) = (\mathbf{r}\mathbf{r}^T - |\mathbf{r}|^2) \exp(-\alpha^2 |\mathbf{r}|^2), \quad (72)$$

to help find a unique orientation. Any three-dimensional molecular integral can now be evaluated as a simple sum

$$\int f(\mathbf{r}) d^3\mathbf{r} \approx \sum_n w_n f(\mathbf{r}_n), \quad (73)$$

where $n = (m, k, i)$ is a combined index.

For a set of atomic basis functions $\{\chi_\mu(\mathbf{r})\}$, their pair product densities

$$q_{\mu\nu}(\mathbf{r}) = \chi_\mu^\dagger(\mathbf{r})\chi_\nu(\mathbf{r}) \quad (74)$$

give rise to the overlap integrals

$$S_{\mu\nu} = \int q_{\mu\nu}(\mathbf{r}) d^3\mathbf{r} \quad (75)$$

$$\approx \tilde{S}_{\mu\nu} = \sum_n w_n q_{\mu\nu}(\mathbf{r}_n). \quad (76)$$

For the two-electron repulsion integrals

$$V_{\kappa\lambda\mu\nu} = \int \frac{q_{\kappa\lambda}(\mathbf{r}_1)q_{\mu\nu}(\mathbf{r}_2)}{|\mathbf{r}_1 - \mathbf{r}_2|} d^3\mathbf{r}_1 d^3\mathbf{r}_2 \quad (77)$$

$$\approx \tilde{V}_{\kappa\lambda\mu\nu} = \sum_n w_n q_{\kappa\lambda}(\mathbf{r}_n) v_{\mu\nu}(\mathbf{r}_n), \quad (78)$$

the seminumerical integration using the analytically computed potentials

$$v_{\mu\nu}(\mathbf{r}) = \int \frac{q_{\mu\nu}(\mathbf{r}_2)}{|\mathbf{r} - \mathbf{r}_2|} d^3\mathbf{r}_2 \quad (79)$$

is at the heart of the fast electronic structure methods we want to use. The integral errors,

$$\varepsilon_S = \max_{\mu\nu} \left| \tilde{S}_{\mu\nu} - S_{\mu\nu} \right|, \quad (80)$$

$$\varepsilon_V = \max_{\kappa\lambda\mu\nu} \left| \tilde{V}_{\kappa\lambda\mu\nu} - V_{\kappa\lambda\mu\nu} \right|, \quad (81)$$

should be small and controllable. If Eq. (78) were used as written, the long-range nature of Coulomb interaction would lead to an error in the molecular energy growing quadratically with its size — even though a very fine integration grid may make it small enough, a smarter way to bring it down to linear is by replacing² the densities on the grid $q_{\kappa\lambda}(\mathbf{r}_n)$ with their ‘‘corrected’’ counterparts

$$\tilde{q}_{\kappa\lambda}(\mathbf{r}) = \chi_\kappa(\mathbf{r})\chi_{\lambda'}(\mathbf{r})Z_{\lambda'\lambda}, \quad (82)$$

$$\mathbf{Z} = \tilde{\mathbf{S}}^{-1}\mathbf{S}, \quad (83)$$

that yield the exact overlap integrals when summed up over the grid points. We have found the symmetric correction

$$\bar{q}_{\kappa\lambda}(\mathbf{r}) = \chi_{\kappa'}(\mathbf{r})\chi_{\lambda'}(\mathbf{r})O_{\kappa'\kappa}O_{\lambda'\lambda}, \quad (84)$$

$$\mathbf{O} = \tilde{\mathbf{S}}^{-1/2}\mathbf{S}^{1/2}, \quad (85)$$

to work no less well, having a good property $\bar{q}_{\lambda\kappa}(\mathbf{r}) = \bar{q}_{\kappa\lambda}(\mathbf{r})$, unlike $\tilde{q}_{\kappa\lambda}(\mathbf{r})$, which may make them easier to handle. Another way to get rid of the quadratic error growth is to rearrange the electrostatic terms by adding and subtracting some promolecule density so that only the Coulomb potential of the deformation density

$$J^d(\mathbf{r}) = \sum_{\mu\nu} v_{\mu\nu}(\mathbf{r})D_{\mu\nu} - \sum_k v_k(\mathbf{r})d_k \quad (86)$$

is handled by the seminumerical integration

$$\tilde{J}_{\mu\nu}^d = \sum_n w_n q_{\mu\nu}(\mathbf{r}_n) J^d(\mathbf{r}_n), \quad (87)$$

where $D_{\mu\nu}$ is the molecular density matrix, and $v_k(\mathbf{r})$ are potentials of simple (such as Gaussian) atom-centered unit-charge distributions with coefficients d_k on each atom adding up to neutralize the nuclear charge, we would readily take these from the optimized effective-potential work²⁷ to further minimize the errors.

Now, back to the problem of spherical quadrature orders L_{ki} in Eqs. (66) and (66), our best solution is an adaptive selection based on the convergence with L of the surface integrals

$$S_{\mu\nu,Lki} = \frac{1}{d_k} \sum_m w_{mLki} q_{\mu\nu}(\mathbf{r}_{mLki}) v(\mathbf{r}_{mLki}), \quad (88)$$

estimated from the differences

$$\mathcal{E}_{\mu\nu,Lki} = |S_{\mu\nu,L+L_1,ki} - S_{\mu\nu,Lki}|. \quad (89)$$

The simplest error measure would have been

$$\mathcal{E}_{Lki} = \max_{\mu\nu} \mathcal{E}_{\mu\nu,Lki}, \quad (90)$$

but we want it to be rotationally-invariant, so we average it over the blocks to get

$$\bar{\mathcal{E}}_{Lki} = \max_{\bar{\mu}\bar{\nu}} \sqrt{\frac{\sum_{m_{\bar{\mu}}m_{\bar{\nu}}} \mathcal{E}_{m_{\bar{\mu}}m_{\bar{\nu}},\bar{\mu}\bar{\nu},Lki}^2}{2 \min(l_{\bar{\mu}}, l_{\bar{\nu}}) + 1}}, \quad (91)$$

where the combined index $\mu = (m_{\mu}, l_{\mu}, n_{\mu}, i_{\mu})$ is split into $m_{\bar{\mu}}$ and $\bar{\mu} = (l_{\bar{\mu}}, n_{\bar{\mu}}, i_{\bar{\mu}})$. The values of $\bar{\mathcal{E}}_{Lki}$ are computed for the growing L , mostly in steps of $L_1 = 6$, until

$$\bar{\mathcal{E}}_{Lki,ki} \approx \varepsilon. \quad (92)$$

For now, we pick the octahedrally-symmetric spherical grids¹⁹ in the series of orders $L = 3, 5, 7, 9, 11, 15, 17, 19, 21, 23, 29, 31, 35, 41, 47, 53, 59, 65, 71, 77, 83, 89, 95, 101, 107, 113, 119, 125, 131$, having 6, 14, 26, 38, 50, 86, 110, 146, 170, 194, 302, 350, 434, 590, 770, 974, 1202, 1454, 1730, 2030, 2354, 2702, 3074, 3470, 3890, 4334, 4802, 5294, 5810 points, but other choices can be made.

With $v(\mathbf{r}) \equiv 1$ in Eq. (88), we would simply adapt the grids to an accurate evaluation of the overlap integrals,

but then they might not be as good for the two-electron integrals; to model the influence of $v_{\mu\nu}(\mathbf{r}_n)$ in Eq. (78), we take

$$v(\mathbf{r}) = 1 + \sum_i \frac{\exp(-a|\mathbf{r} - \mathbf{R}_i|^2)}{|\mathbf{r} - \mathbf{R}_i|}, \quad (93)$$

and find $a = \frac{1}{4}$ to work well.

We have given our method in full and are ready to test it. To sum it up, it takes as input a molecular geometry $\{\mathbf{R}_i\}$, atomic basis functions of Eqs. (61), (62), (63), and an integration accuracy ε . The values A_i of Eq. (64) and α of Eq. (65) are used to set up the radial quadrature of Eq. (55) with $p = 2, q = \frac{1}{8}, h = (\ln 2)/K$, and $A \equiv A_i$ for each atom, with the point density K from Eq. (60) and the ranges from Eqs. (57), (58), and (59). The power ν of Eq. (41) and the scale σ of Eq. (42) are put into the radial functions $u(r)$ of Eq. (40) from which the normalized atomic weighting functions $W_i(\mathbf{r})$ of Eq. (45) are built. The 3×3 matrices of Eqs. (71) and (72) are diagonalized to get the axes \mathbf{X}_i of the spherical grids within the multicenter cubature of Eqs. (66)–(70); the orders L_{ki} are adaptively selected by testing the convergence of $\bar{\mathcal{E}}_{Lki}$ from Eqs. (91), (88), (89), and (93), until Eq. (92) holds.

III. TESTS

We have tested our integration method on a set of molecules made up of light and heavy atoms, working with an easy-to-use scalar-relativistic approximation²⁸ and optimized sets of atomic basis functions²⁹, at CCSD³⁰ geometries, the results are shown in Table I.

For the three typical input accuracy levels, $\eta \equiv -\log_2 \varepsilon = 16, 24, 32$, the output integral errors ε_S of Eq. (80) and ε_V of Eq. (81) are computed over the whole set of overlap and two-electron integrals and reported alongside the average numbers of grid points per atom. Ideally, we should have had $\varepsilon_S = \varepsilon_V = \varepsilon$, but in practice there is some (hopefully small) difference that characterizes the method.

The example of H_2 shows that the grid point density does depend, but weakly, on the basis set size. On the polyacetylenes as models of extended systems, we see how the atom-centered grids saturate with the chain length, being localized in space as they should be. Crowded molecules need denser angular grids, with roughly up to twice as many points. At the high accuracy end $\varepsilon = 2^{-32}$, our adaptive method may run out of precomputed spherical grids as it has to stop at $L = 131$, and this is also where the round-off errors may start to get the upper hand — but such high accuracy would hardly be needed, and the range $2^{-16} \leq \varepsilon \leq 2^{-24}$ would be enough for most applications. High accuracy comes at a high price, but so is the nature of the problem.

TABLE I. Molecular tests of integration accuracy.

molecule	basis	$\eta = 16$			$\eta = 24$			$\eta = 32$		
		η_S	η_V	n_a	η_S	η_V	n_a	η_S	η_V	n_a
H ₂	L1	16	18	2042	25	27	10260	35	36	35420
	L1a	16	18	2184	26	27	10680	34	37	36368
	L2	15	17	3124	24	25	12546	34	36	38956
	L2a	15	16	3194	24	23	13122	33	35	39702
	L3	14	14	5314	24	23	16830	33	32	46058
	L3a	14	14	5422	24	19	17308	33	27	47230
	L4	13	14	6756	23	21	19964	32	28	50802
CH ₄	L4a	13	14	6816	23	17	20432	32	25	52374
	L1	15	17	4026	22	24	25269	32	34	<i>102215</i>
C ₂ H ₆	L2	15	17	5706	21	24	30470	33	34	<i>112712</i>
	L1	15	17	4556	22	24	36246	30	32	<i>143793</i>
C(CH ₃) ₄	L1	14	17	4888	22	25	40903	30	33	<i>168244</i>
H(CC) ₂ H	L1	14	16	3770	23	24	16772	27	29	53284
H(CC) ₃ H	L1	13	15	3938	23	25	17442	27	29	56199
H(CC) ₄ H	L1	13	15	4026	23	25	17654	27	29	57236
H(CC) ₅ H	L1	13	15	4068	22	25	17732	27	29	57667
Li ₄ F ₄	L1	16	18	5545	23	25	36969	31	33	<i>142057</i>
Cs ₄ I ₄	L1	13	17	6822	23	21	36827	30	27	<i>143221</i>
Fe(C ₅ H ₅) ₂	L1	12	14	5910	21	24	42898	30	32	<i>170116</i>
UO ₃	L1	12	13	7598	21	21	32652	28	28	<i>114061</i>

All ε values are given as negative binary logarithms $\eta = -\log_2 \varepsilon$: for input values $\eta = 16, 24, 32$, the observed accuracy of overlap ε_S and two-electron repulsion ε_V integrals is listed along with the average number of grid points per atom n_a (printed in *italics* when running out of spherical grids with $L \leq 131$). Molecular geometries are from CCSD³⁰/L1^{28,29}.

IV. CONCLUSIONS

The quality measure we have defined helps compare, design, and optimize the weighting functions for multi-center numerical integration in molecules. In this way, we have found a remarkably simple one of Eq. (40) working well, as seen from the tests, and easy to implement with linear system-size scaling, as well as for periodic systems. Together with our radial integration scheme and a few handy fitted functions of accuracy ε and exponent α , it makes a black-box numerical tool for electronic structure calculations.

The seminumerical evaluation of two-electron integrals may be the shortest path to fast and scalable³¹ computation of direct and exchange terms of wavefunction methods — we are working toward its use in long-range-corrected³² density functional calculations — as for the “pure”³³ functionals, we have already upgraded our code¹⁶ with the new weighting functions and are using it to help organic chemists understand reaction mechanisms in synthesis³⁴ and catalysis^{35–37}. We have also implemented the six-dimensional spatial integration of dispersion-correction density functionals³⁸ and it begins being used even to interpret the experimental spectroscopy³⁹.

Those who hold true to the original¹¹ or modified¹⁴ fuzzy Voronoi cells may still find our analysis insightful and enjoy adopting Eq. (37) as a smooth and differentiable alternative to Eq. (35).

SUPPLEMENTARY MATERIAL

The code and data for interactive plotting⁴⁰ of the quadrature order distributions is available.

Appendix A: Analytic fit to distribution of quadrature orders

The order of the spherical quadrature L at distance r from the center, in the presence of the second atom at distance R , for the integration of a set of functions of Eq. (6) with $\alpha_n \geq \alpha$ to an accuracy of ε , is an integer value rounded up from a continuous distribution

$$L(r, R, \alpha, \varepsilon) = \lfloor \frac{1}{2} + \lambda(\alpha r, \alpha R, -\log_2 \varepsilon) \rfloor. \quad (\text{A1})$$

As a function of $\eta \equiv -\log_2 \varepsilon$, we find

$$\lambda(s, t, \eta) = \lambda_3(\eta, \kappa(s, t), \gamma(s, t), \beta(s, t)), \quad (\text{A2})$$

$$\lambda_3(\eta, \kappa, \gamma, \beta) = \max \left(0, \frac{\kappa}{\gamma} \left(\exp(\gamma(\eta - \beta)) - 1 \right) \right), \quad (\text{A3})$$

to be a rather good fit, even when constrained to $\gamma \geq 0$, and so we further need the three functions of only two variables $s \equiv \alpha r$ and $t \equiv \alpha R$, for which we take

$$\kappa(s, t) = \kappa_9(a_\kappa(t)s, c_0(t), \dots, c_4(t), p_\kappa(t), u_\kappa(t), v_\kappa(t)), \quad (\text{A4})$$

$$\begin{aligned} \kappa_9(x, c_0, c_1, c_2, c_3, c_4, p, u, v) \\ = \frac{c_0 + c_1 x + c_2 x^2 + c_3 x^3 + c_4 x^4}{(1 + p(x - u)^2)(1 + (x - v)^2/p)}, \end{aligned} \quad (\text{A5})$$

$$\gamma(s, t) = \gamma_4 \left(\frac{s}{s_\gamma(t)} - 1, c_\gamma(t), a_\gamma(t), b_\gamma(t) \right), \quad (\text{A6})$$

$$\gamma_4(x, c, a, b) = \frac{c(a + b)}{b \exp(ax) + a \exp(-bx)}, \quad (\text{A7})$$

$$\beta(s, t) = \beta_7(s, w_\beta, q_\beta(t), b_0(t), b_1(t), b_2(t), d_\beta(t), a_\beta(t)), \quad (\text{A8})$$

$$\begin{aligned} \beta_7(s, w, q, b_0, b_1, b_2, d, a) = -w \ln \frac{s}{\sqrt{s^2 + q^2}} \\ + b_0 + b_1 s + (b_2 s)^2 + d \exp(-as), \end{aligned} \quad (\text{A9})$$

and now for the twenty functions of one variable t , we take w_β as a constant and

$$c_i(t) = c_{c_i} + \frac{d_{c_i}}{1 + \exp(-a_{c_i}(t - t_{c_i}))}, \quad i = 0, 1, 2, \quad (\text{A10})$$

$$c_i(t) = c_{c_i} + b_{c_i} t + \frac{d_{c_i}}{1 + \exp(-a_{c_i}(t - t_{c_i}))}, \quad i = 3, 4, \quad (\text{A11})$$

$$p_\kappa(t) = c_{p_\kappa} + \frac{d_{p_\kappa}}{1 + \exp(-a_{p_\kappa}(t - t_{p_\kappa}))}, \quad (\text{A12})$$

$$u_\kappa(t) = c_{u_\kappa} + \frac{d_{1u_\kappa}}{1 + \exp(-a_{1u_\kappa}(t - t_{1u_\kappa}))} + \frac{d_{2u_\kappa}}{1 + \exp(-a_{2u_\kappa}(t - t_{2u_\kappa}))}, \quad (\text{A13})$$

$$v_\kappa(t) = c_{v_\kappa} + a_{v_\kappa}t, \quad (\text{A14})$$

$$a_\kappa(t) = \frac{c_{a_\kappa} + d_{a_\kappa} \exp(-a_{a_\kappa}t)}{t}, \quad (\text{A15})$$

$$c_\gamma(t) = c_{c_\gamma} + \frac{d_{c_\gamma}}{1 + \exp(a_{c_\gamma}(t - t_{c_\gamma}))}, \quad (\text{A16})$$

$$a_\gamma(t) = c_{a_\gamma} + \frac{d_{a_\gamma}}{a_{a_\gamma}} \ln\left(1 + \exp(a_{a_\gamma}(t - t_{a_\gamma}))\right), \quad (\text{A17})$$

$$b_\gamma(t) = c_{b_\gamma} + d_{b_\gamma} \exp(-a_{b_\gamma}t), \quad (\text{A18})$$

$$s_\gamma(t) = \frac{a_{s_\gamma}t}{\left(1 + (a_{s_\gamma}t/c_{s_\gamma})^8\right)^{1/8}}, \quad (\text{A19})$$

$$b_0(t) = \bar{b}_0(a_{b_0}t), \quad (\text{A20})$$

$$\bar{b}_0(x) = \frac{c_{0b_0} + c_{1b_0}x + c_{2b_0}x^2 + c_{3b_0}x^3 + c_{4b_0}x^4}{1 + d_{b_0}x + x^2}, \quad (\text{A21})$$

$$b_1(t) = -w_{b_1} \ln t + c_{b_1} + \frac{d_{b_1}(a_{b_1} + b_{b_1})}{b_{b_1} \exp(a_{b_1}(t - t_{b_1})) + a_{b_1} \exp(-b_{b_1}(t - t_{b_1}))}, \quad (\text{A22})$$

$$b_2(t) = c_{b_2} + \frac{d_{b_2}}{1 + \exp(a_{b_2}(t - t_{b_2}))}, \quad (\text{A23})$$

$$d_\beta(t) = c_{d_\beta} + \frac{d_{d_\beta}}{1 + \exp(-a_{d_\beta}(t - t_{d_\beta}))}, \quad (\text{A24})$$

$$a_\beta(t) = t_{a_\beta}/t, \quad (\text{A25})$$

$$q_\beta(t) = a_{q_\beta}t. \quad (\text{A26})$$

All the 75 parameters shown in Table (II) are optimized for $\log_2 \alpha = -\frac{9}{2}$ (as an estimate of $\alpha \rightarrow 0$) on a three-dimensional table of values (given in the supplementary material) for $\eta = 6, \dots, 36$ in steps of 1, $\{r_k\}$ of

TABLE II. Parameters of the fitted function $\lambda(s, t, \eta)$ of Eqs. (A2)–(A26).

param.	value	param.	value
c_{c_0}	0.668676279	c_{c_γ}	0.0242344273
d_{c_0}	186.641143	d_{c_γ}	0.00551760331
a_{c_0}	0.811747781	a_{c_γ}	1.46148448
t_{c_0}	7.91647624	t_{c_γ}	1.32454270
c_{c_1}	1.08222907	c_{a_γ}	0.0677721947
d_{c_1}	-357.497539	d_{a_γ}	33.0723100
a_{c_1}	1.04815549	a_{a_γ}	1.47695611
t_{c_1}	7.29100798	t_{a_γ}	8.71490344
c_{c_2}	-2.38602515	c_{b_γ}	18.6441594
d_{c_2}	366.348638	d_{b_γ}	1.10579589
a_{c_2}	1.12810997	a_{b_γ}	0.478453287
t_{c_2}	7.24506698	a_{s_γ}	0.667913966
c_{c_3}	1.36035206	c_{s_γ}	4.10526088
d_{c_3}	-0.370781147	w_β	5.13862547
a_{c_3}	-167.262891	c_{0b_0}	0.789609734
t_{c_3}	1.18103821	c_{1b_0}	4.10945429
c_{c_3}	7.25207491	c_{2b_0}	-11.6359735
d_{c_3}	0.228585146	c_{3b_0}	-8.17218131
b_{c_4}	0.0772105404	c_{4b_0}	4.73484405
d_{c_4}	28.1888933	d_{b_0}	-1.66480653
a_{c_4}	1.22619196	a_{b_0}	0.169755366
t_{c_4}	7.27043411	w_{b_1}	0.691117413
c_{p_κ}	0.350950380	c_{b_1}	-2.53307029
d_{p_κ}	-0.134561547	d_{b_1}	13.3158093
a_{p_κ}	1.71544291	a_{b_1}	0.0619037945
t_{p_κ}	2.07928644	b_{b_1}	0.929786879
c_{u_κ}	0.424179982	t_{b_1}	7.05430131
d_{1u_κ}	2.53098530	c_{b_2}	-0.0247806394
d_{2u_κ}	-4.78594889	d_{b_2}	1.02341270
a_{1u_κ}	0.947678571	a_{b_2}	1.09338554
a_{2u_κ}	0.976692589	t_{b_2}	4.34679065
t_{1u_κ}	3.24854968	c_{d_β}	8.28469547
t_{2u_κ}	7.14486694	d_{d_β}	128.465198
c_{v_κ}	1.11180008	a_{d_β}	1.37480180
a_{v_κ}	0.124042954	t_{d_β}	5.01229765
c_{a_κ}	2.96116919	t_{a_β}	4.59153158
d_{a_κ}	-0.777060497	a_{q_β}	0.125754657
a_{a_κ}	0.386868702		

Eq. (23) and $\{R_k\}$ of Eq. (24) both with $K = 16$. We want to err on the safe side, and we minimize

$$U = \sum_{i,j,k} v\left((\lambda(s_i, t_j, \eta_k) + 1)^2 - (L_{ijk} + 1)^2\right) \quad (\text{A27})$$

where our own error measure function

$$v(x) = x + \frac{\exp(-hx) - 1}{h} \quad (\text{A28})$$

is used instead of the least-squares $\bar{v}(x) = x^2$, it puts a heavier penalty on $x < 0$ (an exponential growth) than on $x > 0$ (close to linear), we set $h = 4$ and get all $\lambda(s_i, t_j, \eta_k) - L_{ijk} > -\frac{1}{2}$ so that the rounded up approximation of Eq. (A1) is never below the exact table value L_{ijk} .

To verify the integrity of Eqs. (A2)–(A26) and parameters of Table (II), and to help implement them, a `gnuplot`⁴⁰ script file for interactive plotting is included in the supplementary material.

Appendix B: Radial quadrature

Here we study the normalized radial functions

$$\varphi_n(r, \alpha) = c_n \alpha^{n+1} r^n \exp(-\alpha^2 r^2), \quad (\text{B1})$$

$$c_0 = \frac{2}{\sqrt{\pi}}, \quad c_1 = 2, \quad c_n = \frac{2c_{n-2}}{n-1}, \quad (\text{B2})$$

with integer $n \geq 0$, as prototypes of atomic and molecular radial distributions to be integrated over r on a grid of points

$$r_k = \rho((k+t)h) \quad (\text{B3})$$

using a coordinate transformation function $\rho(x)$ whose shape can be optimized. The range of α is $0 < \alpha \leq A$, and it can be given as

$$\alpha = A \exp(a) \quad (\text{B4})$$

with $a \leq 0$. The sum

$$S_n(a, t, h) = h \sum_{k=-\infty}^{+\infty} g_n((t+k)h, a), \quad (\text{B5})$$

$$g_n(x, a) = \varphi_n(\rho(x), A \exp(a)) \rho'(x), \quad (\text{B6})$$

approximates the integral and converges to the exact value

$$\lim_{h \rightarrow 0} S_n(a, t, h) = 1, \quad (\text{B7})$$

it is periodic in the shift t ,

$$S_n(a, t+1, h) = S_n(a, t, h), \quad (\text{B8})$$

and the integration error can be defined as the worst case

$$\epsilon_n(a, h) = \max_{0 \leq t \leq 1} |S_n(a, t, h) - 1| \quad (\text{B9})$$

for the given a and h , and further the overall error is

$$\epsilon_n(h) = \max_{a \leq 0} \epsilon_n(a, h). \quad (\text{B10})$$

Very soon, as $h \rightarrow 0$, only the lowest spectral component

$$s_n(a, h) = \int_0^1 S_n(a, t, h) \exp(2\pi i t) dt \quad (\text{B11})$$

is needed, thus

$$\epsilon_n(a, h) \approx \bar{\epsilon}_n(a, h) = 2|s_n(a, h)|. \quad (\text{B12})$$

The integral in Eq. (B11) together with the sum in Eq. (B5) can be unfolded to get

$$s_n(a, h) = \int_{-\infty}^{+\infty} g_n(x, a) \exp\left(\frac{2\pi}{h} i x\right) dx. \quad (\text{B13})$$

Now we are ready for work.

First, we take the simplest and most natural function

$$\rho(x) = \frac{1}{A} \exp(x), \quad (\text{B14})$$

so that the integrand

$$g_n(x, a) = c_n \exp\left((n+1)(a+x) - \exp(2(a+x))\right) \quad (\text{B15})$$

becomes a function only of $a+x$, thus the error $\epsilon_n(a, h)$ of Eq. (B9) is the same for all a , and we can put $a = 0$ and drop it henceforth. With

$$\omega = \frac{2\pi}{h} = \frac{2\pi K}{\ln 2}, \quad (\text{B16})$$

Eq. (B13) becomes

$$s_n(\omega) = c_n \int_{-\infty}^{+\infty} \exp((n+1+i\omega)x - \exp(2x)) dx \quad (\text{B17})$$

and, changing variable from x to $\exp(2x)$, it can be expressed in terms of the gamma function,

$$s_n(\omega) = \frac{c_n}{2} \Gamma\left(\frac{n+1+i\omega}{2}\right), \quad (\text{B18})$$

whose well-known asymptotics

$$\lim_{|z| \rightarrow \infty} \ln \Gamma(z) = \left(z - \frac{1}{2}\right) \ln z - z + \frac{1}{2} \ln(2\pi) \quad (\text{B19})$$

helps us get the long-sought-after answer:

$$-\log_2 \epsilon_0 \approx \frac{\pi^2 K}{2 \ln^2 2} - \frac{3}{2}, \quad (\text{B20})$$

$$-\log_2 \epsilon_1 \approx \frac{\pi^2 K}{2 \ln^2 2} - \frac{1}{2} \log_2 \frac{\pi^2 K}{\ln 2} - \frac{3}{2}, \quad (\text{B21})$$

$$-\log_2 \epsilon_n \approx -\log_2 \epsilon_{n-2} - \log_2 \sqrt{1 + \left[\frac{2\pi K}{(n-1) \ln 2}\right]^2}. \quad (\text{B22})$$

It is the constant of $\frac{3}{2}$ in Eq. (B20) we saw after having solved Eq. (B9) numerically and fitting a straight line through the points that made us believe in the existence of the closed-form expression, it is remarkable how closely Eqs. (B20), (B21), and (B22) fit the exact solutions of Eq. (B9) with Eq. (B14) — for a given error ϵ and a range of n , the almost linear functions $\epsilon_n(K)$ are easy to invert numerically to get the grid point density per octave K .

Now, we take the function

$$\rho(x) = \frac{1}{A} \exp(x - q \exp(-px)) \quad (\text{B23})$$

that gives a double-exponential decay of the integrand

$$\begin{aligned} g_n(x, a, p, q) &= c_n \exp\left[(n+1)(a+x - q \exp(-px))\right] \\ &\times \exp\left[-\exp\left(2(a+x - q \exp(-px))\right)\right] \\ &\times (1 + pq \exp(-px)) \end{aligned} \quad (\text{B24})$$

at both ends,

$$\lim_{x \rightarrow +\infty} g_n = c_n \exp[(n+1)(a+x) - \exp(2(a+x))], \quad (\text{B25})$$

$$\lim_{x \rightarrow -\infty} g_n = c_n p q \exp[-px - (n+1)q \exp(-px)], \quad (\text{B26})$$

and we want to optimize its parameters $p, q > 0$. Whenever $q > 0$, the error $\epsilon_n(a, h, p, q)$ of Eq. (B9) is a non-constant function of a whose values for some $a \approx 0$ are greater than when $q = 0$, the above case of Eq. (B14), but nearly the same as $a \rightarrow -\infty$, so we have to sacrifice some accuracy at one end — however arbitrary it may be, we set the error of Eq. (B10) as

$$\epsilon_n(h, p, q_n(h, p)) = 2\epsilon_n(h, 0, 0) \quad (\text{B27})$$

and thus get an implicit equation for $q_n(h, p) > 0$, what is left is to find a good p . (With Eq. (B24), there seem to be no closed-form solutions for Eqs. (B5), (B9), (B10), and even (B11) — we have to do it all numerically.)

One way to pin down the value of p is by asking for an equal decay rate in Eqs. (B25) and (B26), so we get $p = 2$. Solving Eq. (B27) numerically, we get the values of $q_n(h, 2)$ that oscillate (much for $n = 0, 1$ and less and less for $n > 1$) but seem to have a limit as $h \rightarrow 0$. The case of $n = 0$ stands out as the maximum in Eq. (B10) is at $a < 0$, all $n \geq 1$ seem to have it at $a = 0$. As a rule, we see $q_{n+1}(h, p) > q_n(h, p)$ and they seem to converge with n . To get one q for a given p and all h and n , we need to bracket $q_n(h, p)$ from below, thus we get a pair

$$p = 2, \quad q \approx \frac{1}{8}, \quad (\text{B28})$$

for $n \geq 0$, and a narrower $q \approx \frac{1}{3}$ for $n \geq 1$.

For a full optimization of p and q , we need an objective function, and we define one such by the implicit equation

$$g_n(z_n(h, p), 0, p, q_n(h, p)) = \epsilon_n(h, 0, 0) \quad (\text{B29})$$

and maximize $z_n(h, p)$ over p for a given h to get $p_n(h)$ that yields the fastest decay of the integrand of Eq. (B24) down to ϵ as $x \rightarrow -\infty$. The values of p so calculated oscillate around $p \approx 2$ as $h \rightarrow 0$ for $n = 0$, and slowly grow with $n > 0$ — this only confirms the goodness of Eq. (B28) we now take as our best solution, and the soundness of arguments behind it.

REFERENCES

- ¹W. Kohn and L. J. Sham, Phys. Rev. **140**, A1133 (1965).
- ²R. A. Friesner, J. Chem. Phys. **86**, 3522 (1987).
- ³R. A. Friesner, J. Phys. Chem. **92**, 3091 (1988).
- ⁴T. J. Martinez and E. A. Carter, J. Chem. Phys. **98**, 7081 (1993).
- ⁵R. B. Murphy, M. D. Beachy, R. A. Friesner, and M. N. Ringnalda, J. Chem. Phys. **103**, 1481 (1995).
- ⁶R. Izsák and F. Neese, J. Chem. Phys. **135**, 144105 (2011).
- ⁷D. Bokhan, S. Bernadotte, and S. Ten-no, Chem. Phys. Lett. **469**, 214 (2009).
- ⁸D. Bokhan and D. N. Trubnikov, J. Chem. Phys. **136**, 204110 (2012).
- ⁹P. M. Boerrigter, G. Te Velde, and J. E. Baerends, Int. J. Quantum Chem. **33**, 87 (1988).
- ¹⁰S. F. Boys and P. Rajagopal, Adv. Quantum Chem. **2**, 1 (1966).
- ¹¹A. D. Becke, J. Chem. Phys. **88**, 2547 (1988).
- ¹²G. Voronoi, J. Reine Angew. Math. **134**, 198 (1908).
- ¹³R. E. Stratmann, G. E. Scuseria, and M. J. Frisch, Chem. Phys. Lett. **257**, 213 (1996).
- ¹⁴H. Laqua, J. Kussmann, and C. Ochsenfeld, J. Chem. Phys. **149**, 204111 (2018).
- ¹⁵M. Franchini, P. H. T. Philipsen, and L. Visscher, J. Comp. Chem. **34**, 1819 (2013).
- ¹⁶D. N. Laikov, Chem. Phys. Lett. **281**, 151 (1997).
- ¹⁷J. Andzelm and E. Wimmer, J. Chem. Phys. **96**, 1280 (1992).
- ¹⁸V. I. Lebedev, USSR Comput. Math. Math. Phys. **16**, 10 (1976).
- ¹⁹V. I. Lebedev and D. N. Laikov, Dokl. Math. **59**, 477 (1999).
- ²⁰P. M. Gill, B. G. Johnson, and J. A. Pople, Chem. Phys. Lett. **209**, 506 (1993).
- ²¹O. Treutler and R. Ahlrichs, J. Chem. Phys. **102**, 346 (1995).
- ²²M. E. Mura and P. J. Knowles, J. Chem. Phys. **104**, 9848 (1996).
- ²³R. Lindh, P.-Å. Malmqvist, and L. Gagliardi, Theor. Chem. Acc. **106**, 178 (2001).
- ²⁴H. Takahasi and M. Mori, Publ. RIMS Kyoto Univ. **9**, 721 (1973).
- ²⁵M. Mitani, Theor. Chem. Acc. **130**, 645 (2011).
- ²⁶S. F. Boys, Proc. R. Soc. A **200**, 542 (1950).
- ²⁷D. N. Laikov and K. R. Briling, Theor. Chem. Acc. **139**, 17 (2020).
- ²⁸D. N. Laikov, J. Chem. Phys. **150**, 061103 (2019).
- ²⁹D. N. Laikov, Theor. Chem. Acc. **138**, 40 (2019).
- ³⁰G. D. Purvis and R. J. Bartlett, J. Chem. Phys. **76**, 1910 (1982).
- ³¹H. Laqua, T. H. Thompson, J. Kussmann, and C. Ochsenfeld, J. Chem. Theory Comput. **16**, 1456 (2020).
- ³²D. N. Laikov, J. Chem. Phys. **151**, 094106 (2019).
- ³³J. P. Perdew, K. Burke, and M. Ernzerhof, Phys. Rev. Lett. **77**, 3865 (1996).
- ³⁴K. R. Briling and D. N. Laikov, Russ. J. Org. Chem. **56**, 569 (2020).
- ³⁵O. Vyhivskiy, D. N. Laikov, A. V. Finko, D. A. Skvortsov, I. V. Zhirkina, V. A. Tafeenko, N. V. Zyk, A. G. Majouga, and E. K. Beloglazkina, J. Org. Chem. **85**, 3160 (2020).
- ³⁶O. Adeyiga and S. O. Odoh, ChemPhysChem **22**, 1101 (2021).
- ³⁷O. Adeyiga, D. Panthi, and S. O. Odoh, Catalysis Science & Technology **11**, 5671 (2021).
- ³⁸O. A. Vydrov and T. van Voorhis, J. Chem. Phys. **133**, 244103 (2010).
- ³⁹A. D. Volosatova, M. A. Lukianova, P. V. Zaslavov, and V. I. Feldman, Phys. Chem. Chem. Phys. **23**, 18449 (2021).
- ⁴⁰T. Williams and C. Kelley, “Gnuplot, an interactive plotting program,” .

¹W. Kohn and L. J. Sham, Phys. Rev. **140**, A1133 (1965).